C. R. Palevol 16 (2017) 655–669

Contents lists available at ScienceDirect

Comptes Rendus Palevol

www.sciencedirect.com

General Palaeontology, Systematics and Evolution

A morphometric mapping analysis of lower fourth deciduous premolar in hominoids: Implications for phylogenetic relationship between *Nakalipithecus* and *Ouranopithecus*

Analyse par cartographie morphométrique de la quatrième prémolaire déciduale inférieure chez les hominoïdes : implications pour les relations phylogénétiques entre Nakalipithecus *et* Ouranopithecus

Wataru Morita[a,1], Naoki Morimoto[b,1], Yutaka Kunimatsu[c], Arnaud Mazurier[d], Clément Zanolli[e], Masato Nakatsukasa[b,*]

[a] *Department of Oral Functional Anatomy, Graduate School of Dental Medicine, Hokkaido University, Hokkaido, Japan*
[b] *Laboratory of Physical Anthropology, Department of Zoology, Graduate School of Science, Kyoto University, Kyoto, Japan*
[c] *Faculty of Business Administration, Ryukoku University, Kyoto, Japan*
[d] *Institut de Chimie des Milieux et Matériaux de Poitiers, UMR 7285, Université de Poitiers, Poitiers, France*
[e] *Laboratoire AMIS, UMR 5288 CNRS, Université Toulouse-3, Toulouse, France*

ARTICLE INFO

Article history:
Received 11 July 2016
Accepted after revision 21 October 2016
Available online 4 February 2017
Handled by Roberto Macchiarelli and Clément Zanolli

Keywords:
Miocene
Hominoid evolution
Micro-CT
3D morphometrics

ABSTRACT

Clarifying morphological variation among African and Eurasian hominoids during the Miocene is of particular importance for inferring the evolutionary history of humans and great apes. Among Miocene hominoids, *Nakalipithecus* and *Ouranopithecus* play an important role because of their similar dates on different continents. Here, we quantify the lower fourth deciduous premolar (dp4) inner morphology of extant and extinct hominoids using a method of morphometric mapping and examine the phylogenetic relationships between these two fossil taxa. Our data indicate that early Late Miocene apes represent a primitive state in general, whereas modern great apes and humans represent derived states. While *Nakalipithecus* and *Ouranopithecus* show similarity in dp4 morphology to a certain degree, the dp4 of *Nakalipithecus* retains primitive features and that of *Ouranopithecus* exhibits derived features. Phenotypic continuity among African ape fossils from Miocene to Plio-Pleistocene would support the African origin of African apes and humans (AAH). The results also suggest that *Nakalipithecus* could have belonged to a lineage from which the lineage of *Ouranopithecus* and the common ancestor of AAH subsequently derived.

Mots clés :
Miocène
Evolution des hominoïdes
Micro-CT
Morphométrie 3D

RÉSUMÉ

Afin de mieux comprendre l'histoire évolutive des humains et des grands singes, il est essentiel de caractériser la signature morphologique des hominoïdes africains et eurasiatiques durant le Miocène. Parmi les hominoïdes miocènes, *Nakalipithecus* et *Ouranopithecus* ont un rôle crucial en raison de leur existence à des dates similaires sur des continents différents.

* Corresponding author.
E-mail address: nakatsuk@anthro.zool.kyoto-u.ac.jp (M. Nakatsukasa).
[1] Contributed equally to this work.

http://dx.doi.org/10.1016/j.crpv.2016.10.004
1631-0683/

Nous quantifions ici la morphologie interne de la quatrième prémolaire déciduale inférieure (dp4) des hominoïdes actuels et éteints par des méthodes de cartographie morphométrique et nous examinons les relations phylogénétiques entre ces deux taxons. Nos données suggèrent que les grands singes du Miocène supérieur initial présentent des caractéristiques primitives en général, tandis que les grands singes actuels et les humains montrent des états plus dérivés. Alors que *Nakalipithecus* et *Ouranopithecus* partagent un certain degré de similarité morphologique de leur dp4, la dp4 de *Nakalipithecus* préserve des caractéristiques primitives, tandis que celle d'*Ouranopithecus* montre des traits plus dérivés. Une continuité phénotypique parmi les fossiles de grands singes africains du Miocène au Plio-Pléistocène semble être compatible avec une origine africaine des grands singes africains et des humains (AAH). Nos résultats suggèrent également que *Nakalipithecus* pourrait avoir appartenu à la lignée à partir de laquelle celle d'*Ouranopithecus* et de l'ancêtre commun AAH proviennent.

1. Introduction

The early Late Miocene is a critical period for the speciation of hominids (great apes and humans). Fossil records indicate that the habitat of the Miocene apes covered Africa and Eurasia, while modern great apes are restricted to Africa and Southeast Asia (Fig. 1). Since Miocene apes were geographically and chronologically widespread, a comparison of African and Eurasian apes while controlling for both time and space is essential to reconstruct the evolutionary history of African great apes and humans (AAH). The fossil record of Miocene apes is increasing but is still very limited, and various questions remain unanswered. A key issue is the taxonomy and phylogeny of the currently known Miocene apes. In this study, we address this issue by focusing on deciduous tooth morphology of two Miocene apes, *Nakalipithecus* and *Ouranopithecus*.

Due to their highly mineralized content, dental tissues generally have a greater chance of survival through fossilization than other body parts. Dental morphology has thus routinely been used for functional, phylogenetic, and taxonomic analyses of fossil hominoids (Gómez-Robles et al., 2012, 2015; Pilbrow, 2007; Skinner et al., 2008, 2009a,b; Suwa et al., 2007, 2009). Analyses of tooth morphology are often limited due to dental wear. Recent nondestructive imaging techniques, however, allow us to access the inner structures of teeth. For example, laboratory microcomputed X-ray tomography (μCT) and synchrotron radiation-based imaging enabled extracting the internal structural signature of the teeth of fossil hominins (e.g., Macchiarelli et al., 2004, 2006, 2009; Skinner et al., 2015; Smith and Tafforeau, 2008; Smith et al., 2007; Zanolli et al., 2014).

Teeth in which wear has not reached the dentine provide intact morphological information in terms of the relief of the enamel–dentine junction (EDJ). The EDJ morphology is particularly important for a number of biological reasons. First, it provides insights into development. The EDJ serves as a proxy of the morphogenetic phase of crown formation, where activator–inhibitor signalling and

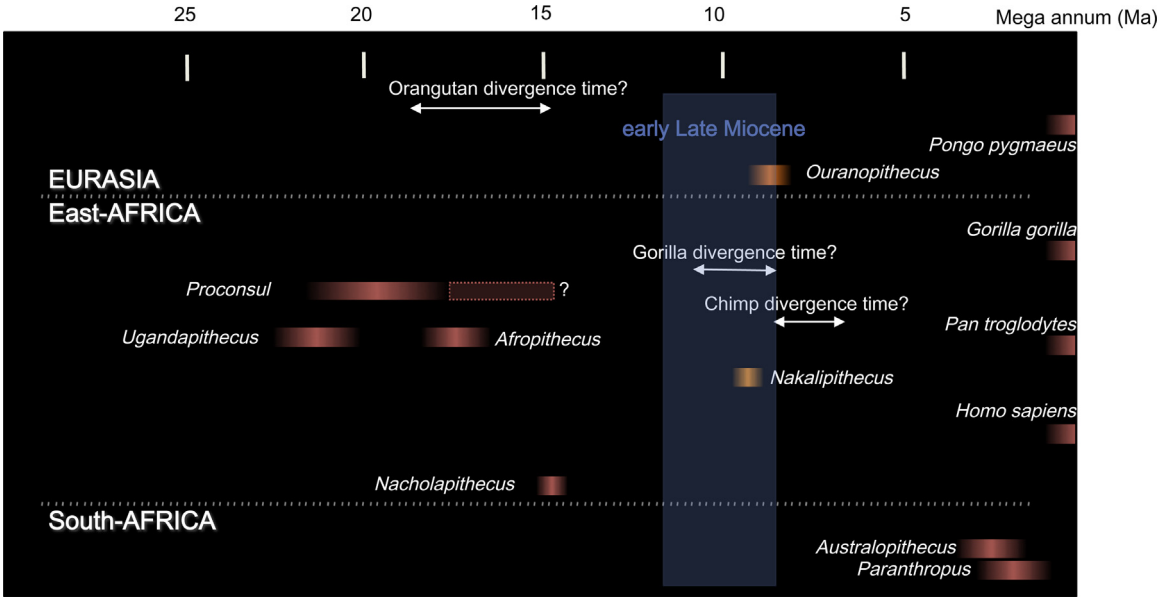

Fig. 1. Chrono-spatial distribution of hominids and large-bodied hominoids used in this study.
Fig. 1. Distribution chrono-spatiale des hominidés et hominoïdes étudiés dans le présent travail.

mechanical interactions occur between the inner enamel epithelium and underlying mesenchymal tissues (Jernvall and Jung, 2000; Jernvall and Thesleff, 2012; Kraus and Jordan, 1965; Morita et al., 2016). Second, the EDJ morphology serves as precursor of the outer enamel surface morphology (Guy et al., 2013; Morita et al., 2014; Skinner et al., 2009a,b), that is then affected by enamel thickness distribution, reflecting dental functions, such as occlusion and feeding. Third, as various studies have indicated, the EDJ morphology is evolutionarily conserved and useful for estimating phylogenetic relationships among fossil hominoids (Korenhof, 1960; Kraus, 1952; Macchiarelli et al., 2006, 2013; Olejniczak et al., 2007; Skinner et al., 2008, 2009a,b, 2010; Smith et al., 1997, 2000; Suwa et al., 2007; Zanolli, 2015; Zanolli and Mazurier, 2013; Zanolli et al., 2014, 2015, 2016).

While the use of the EDJ confers various advantages, the quantitative evaluation of its morphology is challenging. While the landmark-based geometric morphometrics (Bookstein, 1991) provides a strong means to analyze biological shape variation and has been successfully applied to teeth (e.g., Morita et al., 2014; Skinner et al., 2009b, 2016; Zanolli et al., 2012, 2014), it is often extremely difficult to identify the homology between different tooth types and between different taxa. The EDJ is feature-rich and exhibits subtle but variably expressed structures such as the accessory cusps, crests, protostylid or Carabelli's trait. Furthermore, even the same tooth within a same individual (intra-individual) or in conspecific individuals can exhibit great variation. To resolve this problem, the authors developed a new method called morphometric mapping (MM) (Morita et al., 2016). This approach is useful for visualizing and quantitatively analysing the EDJ. Methods of tooth MM have great potential to provide new insights in studies of the Miocene apes.

Using MM, we measure the internal 3D tooth structural morphology of Miocene apes and test two hypotheses that have been proposed about the origin of AAH: the African origin hypothesis (H1) (Katoh et al., 2016) and the Eurasian origin hypothesis (H2) (Begun, 2001, 2010). The former suggests that stem hominids arose in Africa and African Miocene apes gave rise to the lineage of extant gorillas, chimpanzees, and humans, while species expanded into Eurasia lead to Eurasian Miocene apes and modern orangutans. Thus, this hypothesis postulates phyletic continuity between African Miocene apes (whether known or unknown) and extant great apes and humans. On the other hand, the latter hypothesis suggests that extant large hominids originate from a taxon that migrated from Africa to Eurasia approximately 17 Ma. Based on the rarity (*sensu* Hull et al., 2015) of fossil apes from the African Late Miocene, H2 postulates that the common ancestor of AAH arose in Eurasia, migrated back to Africa, and gave rise to the lineages of extant African great apes and humans. The discovery of three African fossil apes, *Samburupithecus*, *Chororapithecus*, and *Nakalipithecus*, from the Late Miocene support the African origin hypothesis (Ishida and Pickford, 1997; Kunimatsu et al., 2007; Suwa et al., 2007; also see Kunimatsu et al., 2016), but no consensus on this issue has yet been reached (Begun, 2005; Begun et al., 2012; Katoh et al., 2016).

Nakalipithecus was recovered from Nakali, Kenya, and dated to 9.9–9.8 Ma (Kunimatsu et al., 2007). The obtained specimens are a partial mandible with worn teeth and several isolated teeth, suggesting that this species had the size of female gorillas and orangutans. The stable isotope analyses and the associated fossils indicate that the local environment was seasonal sclerophyllous evergreen woodlands (C3-dominated). The Nakali primate fauna contains another large-bodied hominoid and other non-cercopithecoid small catarrhines, as well as cercopithecoids such as colobine monkeys (Y.K., unpublished data). Dentally, *Nakalipithecus* resembles *Ouranopithecus* in size and some features but retains less specialized conditions (Kunimatsu et al., 2007).

Ouranopithecus macedoniensis was identified from the early Late Miocene of Greece. It is slightly younger (9.6–8.7 Ma) in chronological age than that at *Nakalipithecus* (Agustí et al., 2001; de Bonis and Melentis, 1977). Based on the morphological similarity in the frontal bone (frontal squama and supraorbital tori), premaxilla (clivus and subnasal fossa), palatine, molar morphology, *Ouranopithecus* is claimed to be similar to the slightly older Eurasian fossil hominoid dryopiths (Begun, 1994, 2002, 2007). It is suggested that *Ouranopithecus* is close to the ancestry of AAH and australopiths (Andrews et al., 1996; de Bonis and Koufos, 1993, 1994, 1997; de Bonis et al., 1990; Koufos, 2007; Koufos and de Bonis, 2004), or that this species underwent convergent evolution as a result of selection for powerful mastication (Begun and Kordos, 1997). However, the phyletic position of this species has not yet been settled (Moyá-Solá and Köhler, 1995). One of the fossil materials that is available for *Nakalipithecus* and *Ouranopithecus* is the lower fourth deciduous premolar (dp4). However, relatively little attention has been paid to deciduous dental morphological variation in the context of Miocene hominid evolution.

Generally, it is accepted that the morphology of deciduous dentition is highly conservative (Butler, 1956, 1971; Dahlberg, 1945; Saunders and Mayhall, 1982; Smith, 1989; Smith and Tillier, 1989; Suzuki and Sakai, 1973) because it directly reflects genetic variation more strongly (less perturbations caused by environmental noise) than the morphology of permanent teeth due to the earlier and more rapid formation during development (Nanci, 2013). Thus, the dp4 is highly stable in terms of size, morphology and timing of emergence and is considered as the key tooth of the deciduous and permanent molar fields (e.g., Bockmann et al., 2010; Bolk, 1916; Butler, 1956, 1971; Saunders and Mayhall, 1982). Recently, the deciduous dentition of fossil hominids has become a focus of some studies (Bailey et al., 2014, 2016; Bayle et al., 2010; Benazzi et al., 2011a,b; Evans et al., 2016; Macchiarelli et al., 2006; Zanolli et al., 2010, 2012).

Applying original techniques to the subtle characters of the dp4 inner structural morphology, we comparatively assessed the structural signal from a multiple morphometric parameters, with the aim of contributing to elucidation of phylogenetic relationships between *Nakalipithecus* and *Ouranopithecus*. We also aim to assess the phylogenetic position of these fossil apes from the early Late Miocene compared with extant hominids and extinct

Mio-Plio-Pleistocene hominoids. If *Nakalipithecus* is closer to older species, then H1 is supported. Alternatively, if *Ouranopithecus* is closer to older species, then H2 is more likely sustained. Specifically, in this study, we analyze the EDJ morphology of dp4 using a novel method, morphometric mapping (MM) (Morimoto et al., 2011, 2012, 2014; Morita et al., 2016; Puymerail et al., 2012) to precisely quantify the complex three-dimensional crown morphology.

2. Materials and methods

The dental sample comprised 46 mandibular dp4s, including *Nakalipithecus* ($N = 1$), *Ouranopithecus* ($N = 1$), Miocene African hominoids ($N = 8$), Plio-Pleistocene australopiths from South Africa ($N = 3$; including gracile and robust australopiths), and extant great apes and humans (*Pan troglodytes*: $N = 6$, *Gorilla gorilla*: $N = 6$, *Pongo pygmaeus*: $N = 7$, *Homo sapiens*: $N = 14$) (Table 1, Fig. 1). Specimens with well-preserved EDJ morphologies were selected for this study (except for the only available *A. africanus* specimen STS 24 for which the apical extremity of the dentine horns was numerically reconstructed). Both right and left teeth were used to maximize the sample size. For most of the samples, the sex was unknown.

Scans of all specimens were undertaken using μCT scanners at a voxel size between 24 and 72.5 μm. Specimens of *Nakalipithecus* and other Miocene African fossils were scanned using a peripheral quantitative CT scanner (pQCT: XCT Research SA +) with a tube voltage of 50 kV, a tube current of 50 μA, and a voxel size of 50 μm. Specimen of *Ouranopithecus* was also scanned at 50 μm (240 kV, 50 μA) with an in-house set-up of the Bundesanstalt für Materialforschung und -Prüfung (BAM) at Berlin (Macchiarelli et al., 2009). Australopiths were scanned using a Nikon XTH 225 ST equipment of the South African Nuclear Energy Corporation (South Africa). Some extant hominids were μCT-scanned using a Viscom X8050-16 system of the University of Poitiers (France) and the rest of the extant great ape specimens were scanned using a ScanXmateA080S μCT scanner with the voxel size 27–63 μm. Micro-computed tomography (μCT) images of left molars were transformed into their mirror images using ImageJ software (National Institutes of Health, Bethesda, MD, USA), and finally, all specimens were regarded as being from the right side. Image segmentation was conducted on each cross section by semi-automatic thresholding methods using Avizo v.6.2 (Visualization Sciences Group Inc., Burlington, MA, USA) and ImageJ software following standard protocols (Coleman and Colbert, 2007; Fajardo et al., 2002; Spoor et al., 1993).

Table 1
Deciduous lower second molars used in this analysis.
Tableau 1
Liste des secondes molaires lactéales inférieures étudiées dans ce travail.

Taxon	Specimens
Nakalipithecus	KNM-NA 46435
Ouranopithecus	RPl 83
Proconsul	KNM-RU 1865
Ugandapithecus	KNM-ME 10
	KNM-LG 1460
	KNM-SO 451
	KNM-RU 1767
Afropithecus	KNM-MO 26
Nacholapithecus	KNM-BG 15331
	KNM-BG 15334
Australopithecus	Sts 24
Paranthropus	SK 61
	SK 63
Homo	($N = 14$)
Pan	($N = 6$)
Gorilla	($N = 6$)
Pongo	($N = 7$)

A three-dimensional surface model was generated from segmented images. First, the outline of the cusp tip and intercuspal ridges of each tooth was manually digitized on the surface model using MeshLab 1.3.3 software (http://meshlab.sourceforge.net/), and the least-squares plane of the occlusal table was computed. Each deciduous premolar was then positioned with the least-squares plane parallel to the *xy*-plane of the Cartesian coordinate system and centred on the centroid of the occlusal table. Then, the *xy*-plane shifts to a cervical plane that was calculated from the digitized cervical line.

In this study, the following three morphometric parameters were used: the mean curvature of the EDJ surface (c) was calculated analytically for each vertex of the 3D model, whereas the height from the cervical plane (h) and the radius from the centroid of the cervical line (r) were calculated directly from the 3D coordinates of the surface mesh. These three parameters represent the following morphological features: c, surface relief; h, height and relative positions of cusps; r, relative diameter in a horizontal direction.

For each specimen, these three variables (c, h, and r) were sampled from each cross-sectional outline and around the entire EDJ surface. The EDJ surface was digitally sectioned equiangularly ($L = 300$) by a plane orthogonal to the *xy*-plane and through the centroid. In each cross section, the outline that runs from the point located just above the centroid of the coordinate system to the point at the level of the *xy*-plane (equal to cervix) was parameterized by elliptic Fourier analysis (EFA) equidistantly ($K = 300$). EFA was used to reduce noise and define parametric outline functions (Kuhl and Giardina, 1982). They were mapped onto a polar coordinate system (d, θ), where d denotes the normalized position along each cross-sectional outline ($d = 0 \rightarrow 1$: centroid→cervix) and θ denotes the anatomical direction [$\theta = 0^\circ \rightarrow 360^\circ$: buccal ($0^\circ$)→mesial ($90^\circ$)→lingual ($180^\circ$)→distal ($270^\circ$)→buccal ($360^\circ$)]. The EDJ could be visualized using 2D morphometric maps M (d, θ), and the distributions c (d, θ), h (d, θ), and r (d, θ) could be represented as $K \times L$ matrices, where K and L denote the numbers of elements along d and θ, respectively ($K = L = 300$).

The effects of scaling were corrected by normalization of the variables c, h, and r using cervical size (i.e., the square root of the summed squared distances of each value of r at the cervix [$d = 300$]). This is analogous to the ordinary geometric morphometric method (Bookstein, 1991). Each row of the $K \times L$ matrix for each specimen was weighted by the length of each cross-sectional outline and the value of r for each element.

For the comparative analysis of the morphometric maps M_i of all specimens ($i = 1, 2, \ldots, N$), differences between specimens in orientation around the centroid (θ) had to be minimized. First, all specimens were pre-aligned manually to orient them in an anatomical direction similar to that described above. Second, optimal fitting was achieved by iteratively minimizing inter-specimen distance in Fourier space through rotation around θ (z-axis). Furthermore, 2D-Fourier transforms $F(M_i)$ of all M_i were calculated (M has natural periodicity in θ), resulting in $K \times L$ sets of Fourier coefficients that represented a specimen's shape of the EDJ surface as a point in the multidimensional Fourier space. Major patterns of shape variation among fossil and extant specimens were inspected using principal component analysis (PCA) on the low-frequency domain of Fourier coefficients (i.e., low-pass filtering in Fourier space [see Morita et al., 2016, for details]) of the mean configurations of extant genera (i.e., the eigen analysis was carried out on the group means) employing the covariance matrix. To take into account the intraspecific variation of the extant samples, PC scores for all of the original individuals were computed *a posteriori* using vector products. This method is also called between-group PCA (bgPCA) (Almécija et al., 2013; Gunz et al., 2012; Mitteroecker and Bookstein, 2011). To facilitate visual inspection and morphological interpretation of the results of bgPCA, morphometric maps were reconstructed by transforming an arbitrary point in bgPC space into its corresponding sets of Fourier coefficients and then applying an inverse transformation. Morphometric maps were visualized

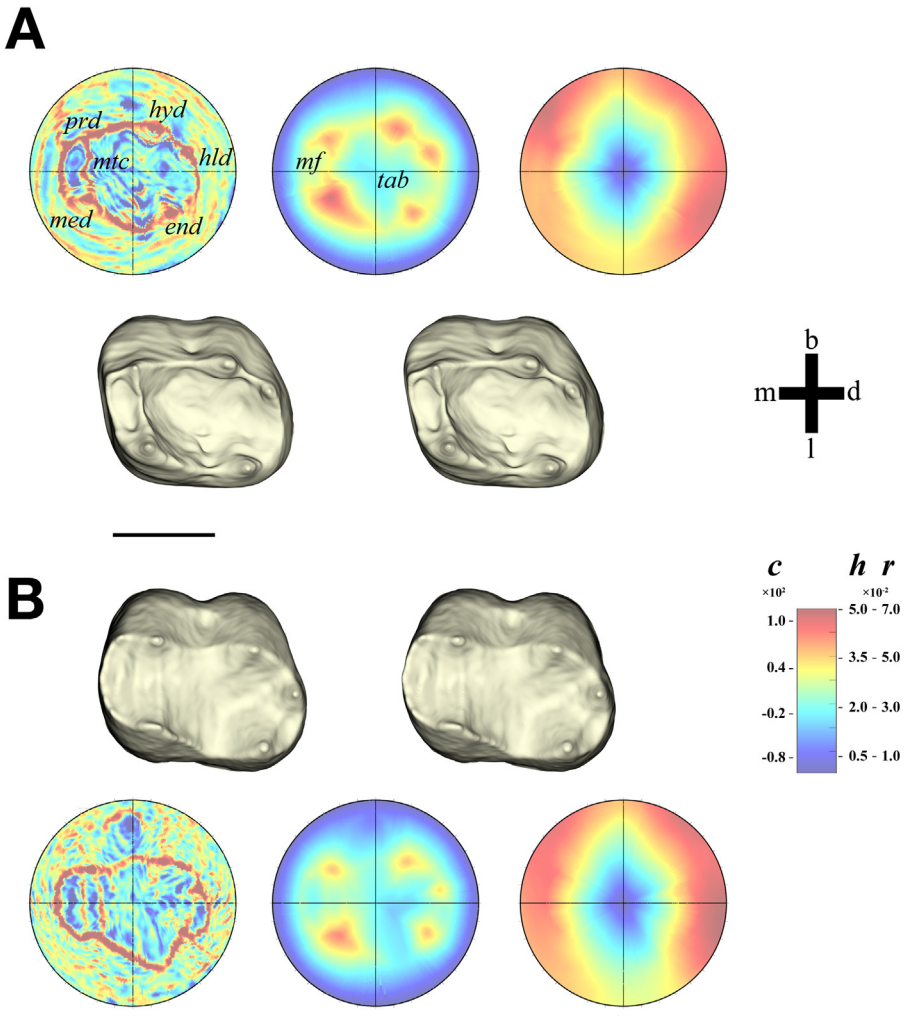

Fig. 2. Three-dimensional model of the enamel–dentine junction (stereo picture) and corresponding morphometric maps [surface curvature (c), height from the cervical line (h), and radius from the centroid of the occlusal table (r), from left to right] of *Nakalipithecus* (mirrored from original specimen) (A) and *Ouranopithecus* (B). Scale bar: 5 mm. *prd*: Protoconid, *med*: metaconid, *mtc*: mesial transversal crest, hyd: hypoconid, *end*: entoconid, *hld*: hypoconulid, *mf*: mesial fovea, *tab*: talonid basin, b: buccal, m: mesial, l: lingual, d: distal.

Fig. 2. Modèle en trois dimensions de la jonction émail–dentine (image stéréo) et cartes morphométriques correspondantes [la courbure de surface (c), la hauteur de la ligne cervicale (h), et le rayon depuis le centroïde de la surface occlusale (r), sont indiqués de gauche à droite] de *Nakalipithecus* (symétrique du spécimen original) (A) et *Ouranopithecus* (B). Barre d'échelle : 5 mm. *Prd :* Protoconide, *med :* métaconide, *mtc :* crête transversale mésiale, *hyd :* hypoconide, *end :* entoconide, *hld :* hypoconulide, mf : fovéa mésiale, *tab :* bassin du talonide, b : buccal, m : mésial, l : lingual, d : distal.

using a false-colour mapping scheme. All calculations were performed in MATLAB 8.1 (MathWorks, Natick, MA, USA) (see Morita et al., 2016, for details). Phenotypic distances among specimens were calculated as Euclidean distances in morphospace. The neighbour-net diagram was computed with SplitsTree4 (Huson and Bryant, 2006). The phylogeny of extant anthropoid taxa was based on the consensus tree downloaded from the 10 kTree website (ver. 3; http://10ktrees.fas.harvard.edu/) (Arnold et al., 2010) and modified with Mesquite v. 3.05 (Maddison and Maddison, 2015) to condense the tips at the generic level. We reconstructed the evolutionary history of dp4 in extant and extinct hominoids by projecting the phylogenetic tree into morphospaces (= bgPC shape space) using the R package "phytools" (Revell, 2012).

3. Results

Fig. 2 shows a visual comparison of the 3D representation of dp4 EDJ morphology and its corresponding MM for *Nakalipithecus* and *Ouranopithecus* specimens. The EDJ surface and MM show marked features that are associated with the characteristics of the enamel surface. Hence, we used anatomical terms for the enamel surface to indicate EDJ features.

In a *Nakalipithecus* specimen (Fig. 2A), MM of the surface curvature (*c*-M) captured well-defined anatomical features: five cusps (protoconid, metaconid, hypoconid, entoconid, and hypoconulid), ridges that are located between the cusps and delimit the occlusal table, and the mesial transverse crest. The *Nakalipithecus* dp4 has

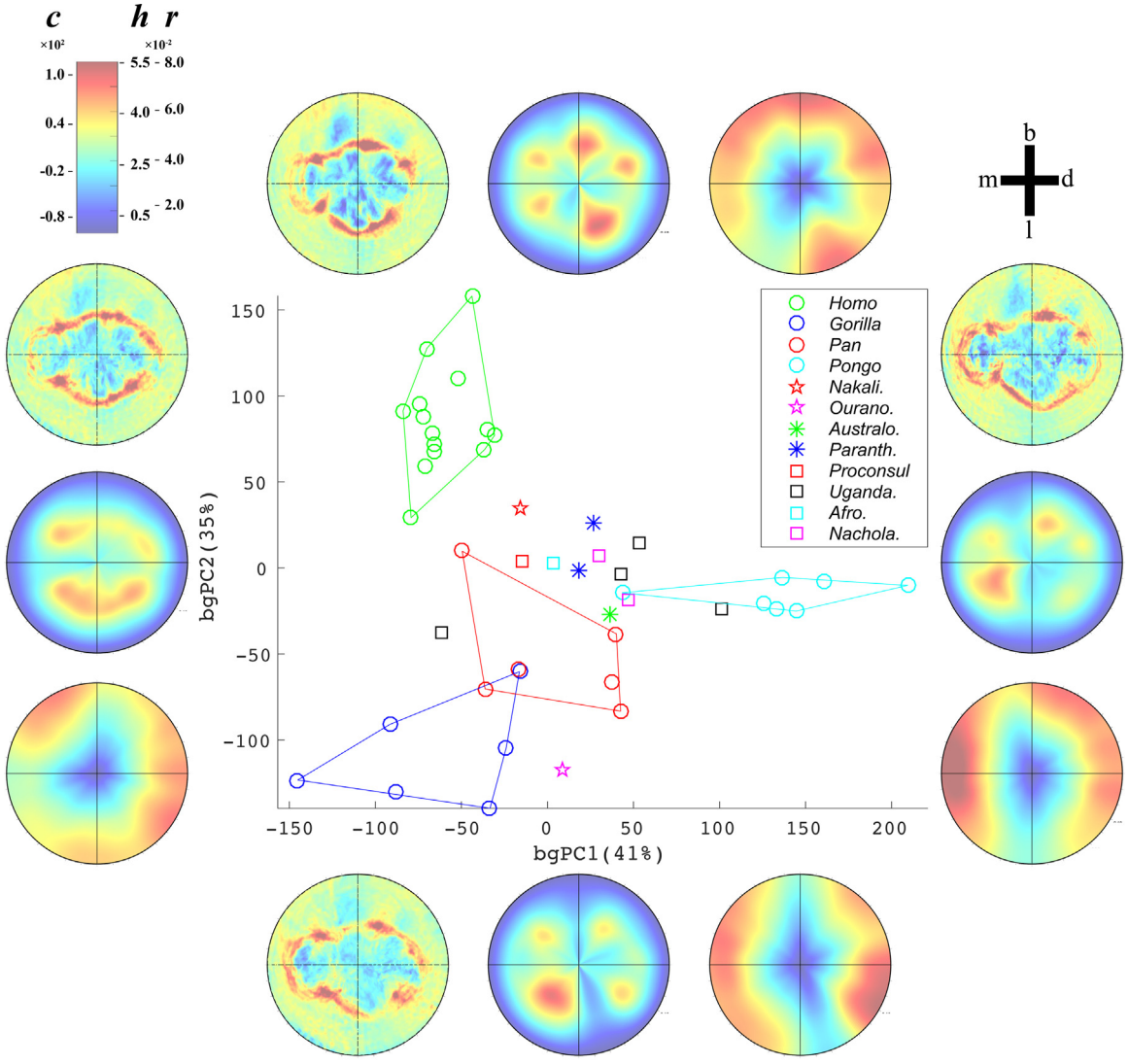

Fig. 3. Variation along between-group principal components (bgPCs) 1 and 2. Morphometric maps (*c*, *h*, and *r*, from top to bottom and left to right) visualizing ±1 s.d. along each bgPC axis. b: Buccal, m: mesial, l: lingual, d: distal.

Fig. 3. Variation le long des composantes principales (bgPCs) 1 et 2 de l'analyse intergroupes. Les cartes morphométriques (*c*, *h*, et *r*, de haut en bas et de gauche à droite) représentent ± 1 écart-type le long de chaque axe bgPC. b : Buccal, m : mésial, l : lingual, d : distal.

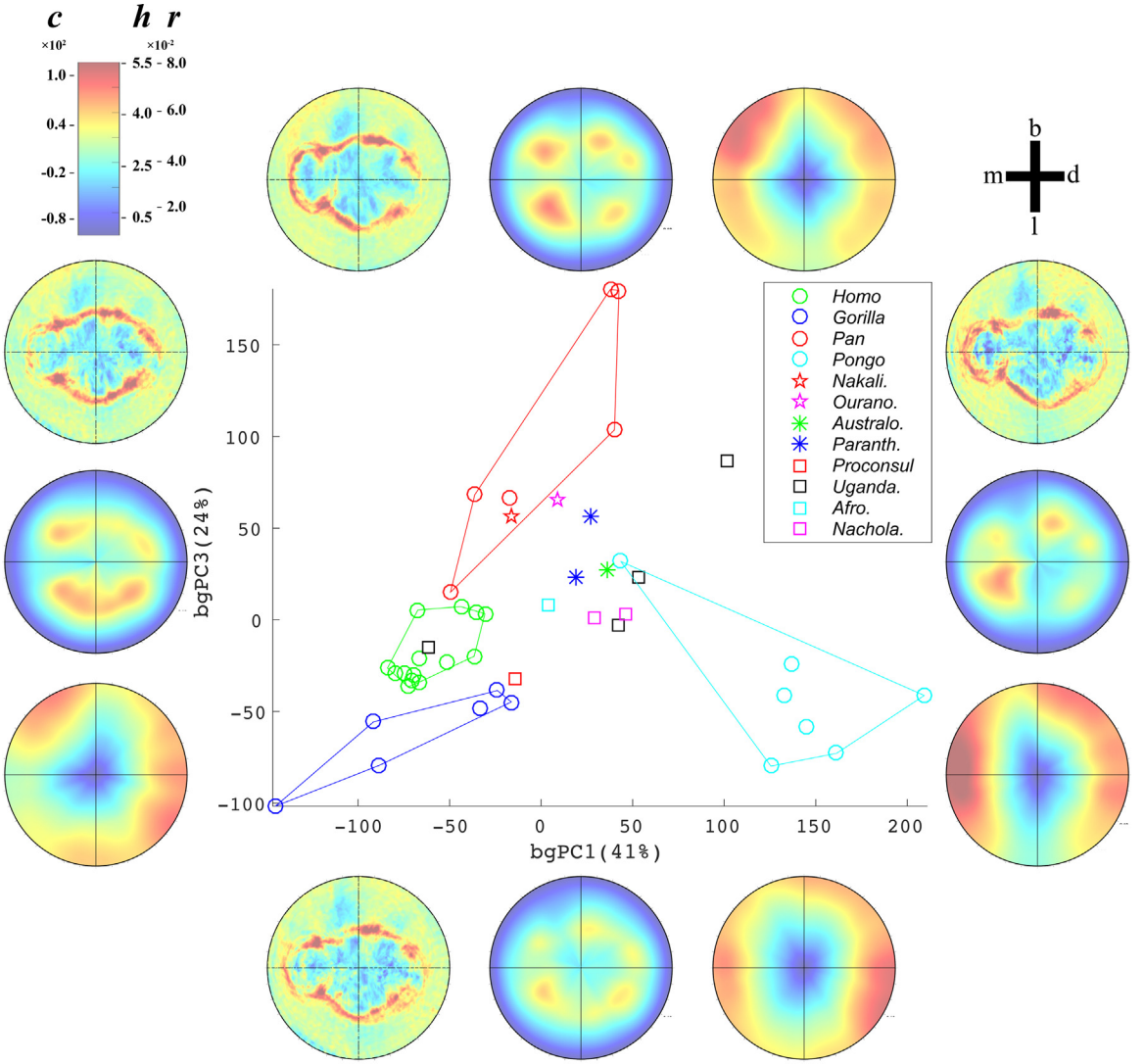

Fig. 4. Variation along between-group principal components (bgPCs) 1 and 3. Morphometric maps (*c*, *h*, and *r*, from top to bottom and left to right) visualizing ±1 s.d. along each bgPC axis. b: buccal, m: mesial, l: lingual, d: distal.
Fig. 4. Variation le long des composantes principales (bgPCs) 1 et 3 de l'analyse intergroupes. Les cartes morphométriques (*c*, *h*, et *r*, de haut en bas et de gauche à droite) représentent ± 1 écart-type le long de chaque axe bgPC. b : Buccal, m : mésial, l : lingual, d : distal.

a weakly developed buccal cingulum, located on the mesiobuccal face of the protoconid and small depressions at the bases of the buccal grooves and at the distobuccal side between the hypoconid and the hypoconulid. MM of height (*h*-M) from the cervix captured the relative location and distribution of the cusps, showing a high and relatively large metaconid, a relatively small mesial fovea and a broad talonid basin. MM of the radius (*r*-M) from the centroid of the cervical line gave a comprehensive view of the horizontal dimensions of the EDJ, showing elongation in mesiobuccal, distobuccal, and distolingual directions.

In an *Ouranopithecus* specimen (Fig. 2B), *c*-M demonstrated five cusps and well-developed ridges between cusps. The mesial fovea is relatively large with a secondary ridge running in the buccolingual direction. A small cingulum and relatively large depression are present on the buccal valley between the protoconid and the hypoconid. The *h*-M showed low cusps relatively to *Nakalipithecus*, especially to the hypoconulid, and a broad talonid. The trigonid and talonid are located distantly. The *r*-M also captured a larger dimension in a distal direction.

MM-based shape variation of the entire sample was explored using bgPCA in which all three bgPC axes were computed (see Supplementary Figs. S1–S6 to see the contribution of each morphometric parameter). In this shape space, extant great apes are well divided from each other (Figs. 3 and 4; see also Supplementary Fig. S7 for a 3D plot). The bgPC1 (41% of variance) largely separates *Pongo* from other hominids. A positive value along bgPC1 is associated with the following features: sharp metaconid and hypoconid and concave mesial fovea (*c*-M); high metaconid and hypoconid (*h*-M); and larger dimension in a mesial direction (*r*-M). A negative value along bgPC1 is associated with the following features: sharp buccal and

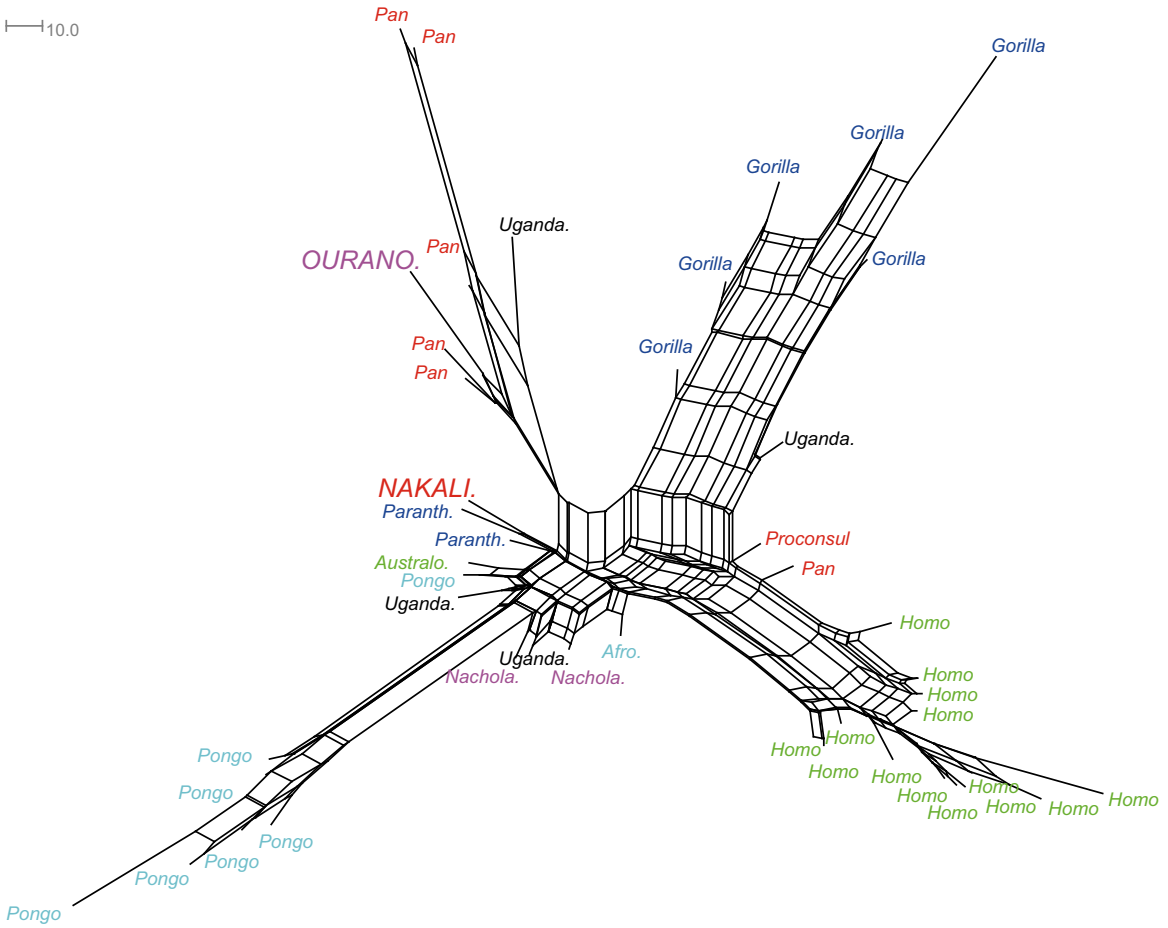

Fig. 5. Neighbour-net diagram of all specimens based on Euclidean distances in morphospace.
Fig. 5. Diagramme *Neighbour-net* de tous les échantillons, en fonction de leur distance euclidienne dans le morpho-espace.

lingual inter-cusp ridges and interrupted occlusal outline at mesial and distal ridges (*c*-M); high protoconid and lingual two cusps (*h*-M); and mesiobuccal–distolingual elongation (*r*-M). The bgPC2 (35% of variance; Fig. 3) captured differences between *Homo* and other hominids from higher and more pointed five cusped dp4s to teeth with less developed hypoconulid. A positive value along bgPC2 is associated with the following features: clear relief, that is, pointed cusps and incised grooves (*c*-M); five well-defined cusps, especially on talonid with higher hypoconid and entoconid (*h*-M); and larger in hypoconid and entoconid directions (*r*-M). On the other hand, the negative value along bgPC2 is associated with the following features: pointed cusps (except for the hypoconulid) and a reduced talonid basin (*c*-M); four cusps with a notably high metaconid and diminished hypoconulid (*h*-M); and larger in a distal direction and constricted at the middle of buccal and lingual side (*r*-M).

Further, bgPC3 (Fig. 4) separates *Pan* from the other taxa. A positive value along bgPC3 (24% of variance) is associated with the following features: sharp in both cusp tips and inter-cusp ridges (*c*-M); higher cusps (*h*-M); and larger in a mesiobuccal direction (*r*-M). Conversely, a negative value along bgPC3 is associated with the following features: lower dentine horns and marginal ridges tips (*c*-M); significantly lower cusps (*h*-M); and larger in a distolingual direction (*r*-M).

Considering the shape space defined by bgPC1 and bgPC2 (Fig. 3), *Nakalipithecus* and *Ouranopithecus* do not overlap with the range of extant great apes. On the other hand, they differ from each other along bgPC2. They occupy close positions in bgPC1 and bgPC3 space (Fig. 4) and are located close to the distribution of *Pan*. Miocene African fossil hominoids as well as Plio-Pleistocene australopiths occupy a general mean position among extant hominids (see also Supplementary Figs. S8 and S9: PC plots with only fossil specimens).

Between-taxon distances were evaluated by calculating the Euclidean distances in morphospace (bgPC1-bgPC3), and distance-based similarity patterns were visualized as a neighbour-net diagram (Fig. 5). Most of the conspecific specimens of extant great apes are connected to each other and form taxon-specific clusters. The clusters of extant great apes are located distant from each other. On the other hand, Early and Middle Miocene African hominids (MAH: *Proconsul*, *Ugandapithecus*, *Afropithecus*,

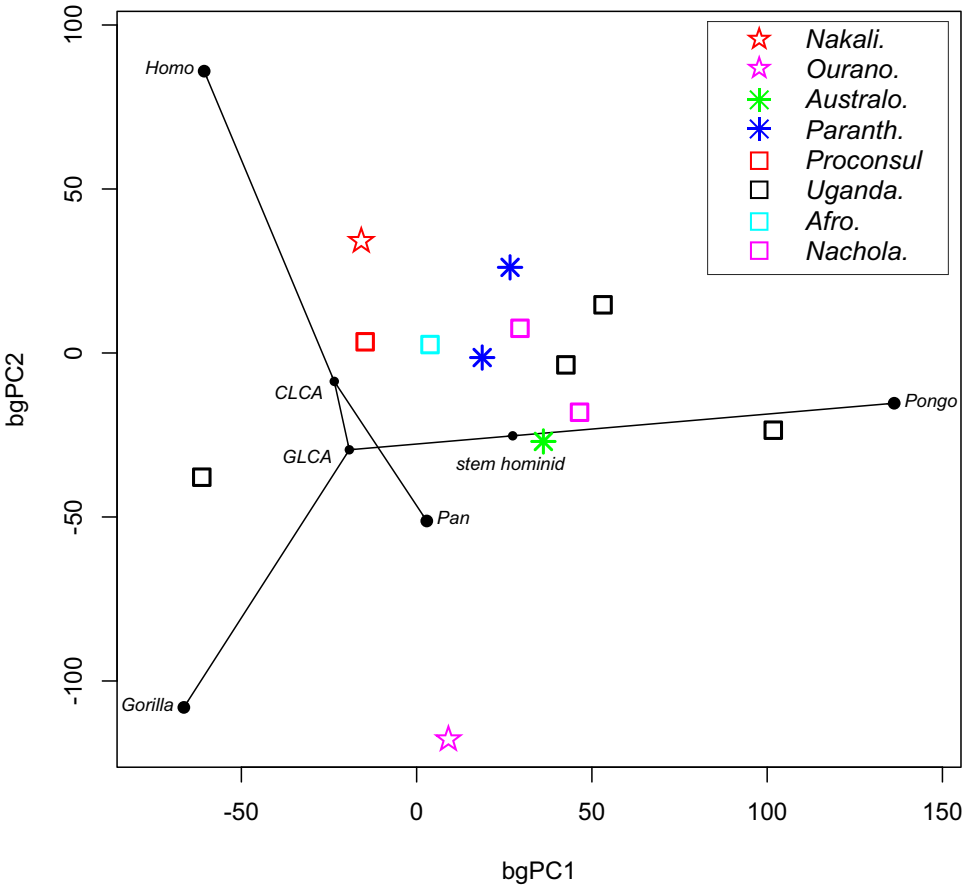

Fig. 6. Phylo-morphospace of hominid dp4s. The phylogeny of extant great apes is projected into a plot defined by between-group principal components (bgPCs) 1 and 2 of the covariance matrix among extant species means. Internal node morphologies [stem hominid, extant African ape and human ancestor (GLCA), and the chimpanzee/human last common ancestor (CLCA)] were reconstructed using squared-change parsimony.
Fig. 6. Espace morpho-phylogénétique des dp4s hominidés. La phylogénie des grands singes actuels est projetée dans une parcelle définie par les composantes principales (bgPCs) 1 et 2 de l'analyse intergroupes basée sur la matrice de covariance entre les moyennes d'espèces existantes. La morphologie des nœuds internes [représentant l'hominidé souche, ancêtre africain des grands singes existants et des humains (GLCA) et le dernier ancêtre commun chimpanzé/humain (CLCA)] a été reconstruite à l'aide de la méthode *squared-change parsimony*.

and *Nacholapithecus*) are located close to the centre of this diagram, except for two *Ugandapithecus* specimens. The *Nakalipithecus* specimen is not located so distant from the centre of this diagram, while the *Ouranopithecus* specimen is situated more peripherally, in the *Pan* cluster.

Fig. 6 (bgPC1 vs. bgPC2) and Fig. 7 (bgPC1 vs. bgPC3) show a phylo-morphospace projection of the phylogeny of extant great apes onto bgPCs of dp4 in extant and fossil species, reconstructing hypothetical ancestral morphologies as internal nodes. MAH are largely located close to the basal node of the great apes (=stem hominid). Plio-Pleistocene australopith specimens are also located close to the basal node. The inferred *Gorilla-Pan-Homo* last common ancestor (GLCA) and *Homo-Pan* last common ancestor (CLCA) are located close to each other. The *Nakalipithecus* specimen is located closer to both GLCA and CLCA than *Ouranopithecus*. Fig. 8 shows the average MM of dp4 EDJ of four extant great ape species, MAH, and the inferred states of stem hominids, GLCA and CLCA. The average shape of *Homo* is characterized by greater surface relief with high talonid cusps, particularly the entoconid, and a large radius in the lingual direction. The average shape of *Pan* is characterized by concave mesial fovea, high and sharp trigonid cusps, and a large diameter in the mesiobuccal direction. The average shape of *Gorilla* is characterized by high and pointed lingual cusps and a large diameter in the distolingual direction with a buccolingual constriction at the middle. The average shape of *Pongo* is characterized by a broad and concave talonid basin, high and mesially located metaconid, and a large diameter in the mesial direction. The average shape of MAH is characterized by five pointed cusps, a narrow and concave mesial fovea, and a large dimension in the mesiobuccal direction associated to a small dimension in the lingual direction. MM of the inferred stem hominid reconstructed from morphospace resembles MAH in exhibiting five well-developed cusps and a concave mesial fovea. The inferred morphologies of GLCA and CLCA are similar to each other, but GLCA exhibits a larger diameter in the distal direction while CLCA has a higher protoconid and entoconid than GLCA.

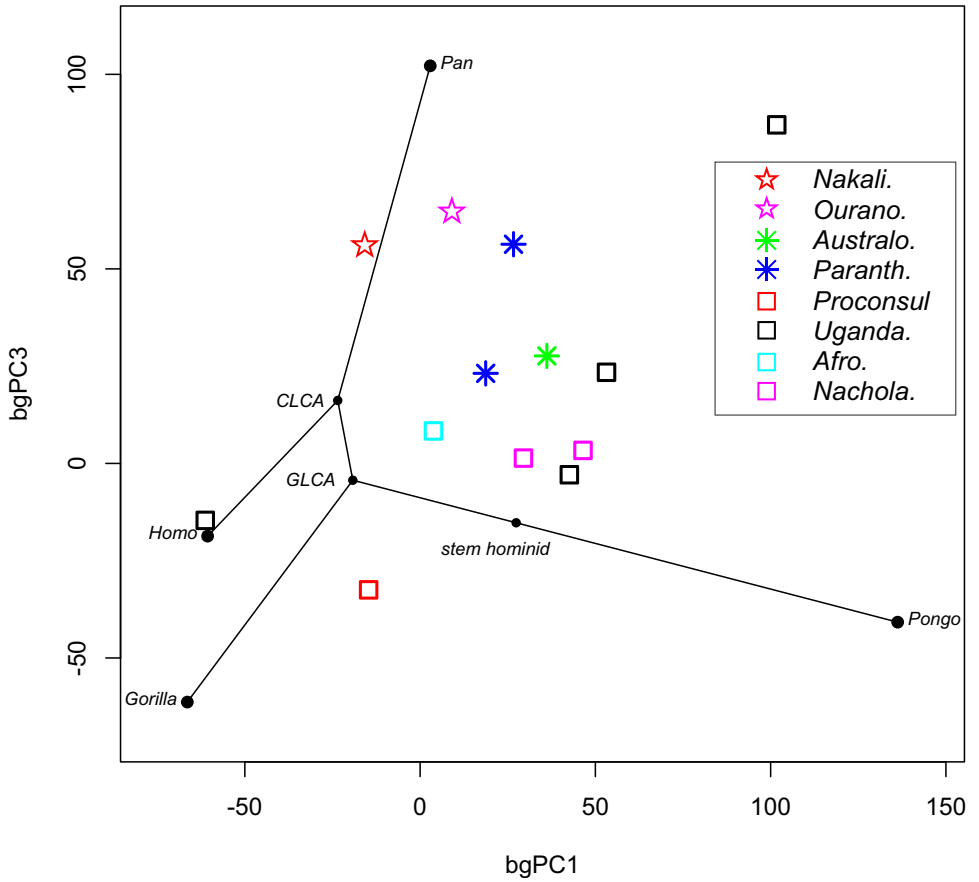

Fig. 7. Phylo-morphospace of hominoid dp4s. The phylogeny of extant great apes is projected into a plot of between-group principal components (bgPCs) 1 and 3. Internal node morphologies [stem hominid, extant African ape and human ancestor (GLCA), and the chimpanzee/human last common ancestor (CLCA)] were reconstructed using squared-change parsimony.

Fig. 7. Espace morpho-phylogénétique des dp4s d'hominidés. La phylogénie des grands singes actuels est projetée dans une parcelle définie par les composantes principales (bgPCs) 1 et 3 de l'analyse intergroupes basée sur la matrice de covariance entre les moyennes des espèces existantes. La morphologie des nœuds internes [représentant l'hominidé souche, ancêtre africain des grands singes existants et des humains (GLCA) et le dernier ancêtre commun chimpanzé/humain (CLCA)] a été reconstruite à l'aide de la méthode squared-change parsimony.

4. Discussion

The data of MM-based PCA showed that the dp4 morphologies of the extant great apes were well divided from each other (Figs. 3 and 4). Most specimens of Miocene African hominoids were located around the grand mean of extant hominids, while extant taxa were located more peripherally in the morphospace. The similarity pattern of living and fossil individuals was also visualized as a neighbour-net diagram (Fig. 5). The neighbour-net diagram showed that Miocene hominoids were located around the central node of the diagram, whereas specimens of extant taxa were located peripherally.

Given that extant great ape taxa exhibit a great degree of diversification and that chronologically distant Plio-Pleistocene hominins and Miocene hominoids exhibit close dp4 morphology, it is not likely that modern great apes retain primitive morphology of the dp4. Alternatively, the analysis of dp4 morphology suggests that modern great apes and humans represent a derived state and that Plio-Pleistocene hominins represent a primitive state retained from Miocene African hominids. This is consistent with the evolutionary scenario proposed in various recent studies of fossil hominins (Almécija et al., 2013, 2015; Lovejoy et al., 2009; Moyá-Solá et al., 2009; Nakatsukasa and Kunimatsu, 2009).

Our results indicate that extant hominids evolved taxon-specific features of dental morphology from the ancestral state in Miocene African hominoids, probably reflecting taxon-specific adaptations, for example, a preference for ripe fruit in *Pan* (Janmaat et al., 2016; Yamagiwa and Basabose, 2006) and folivory with seasonal frugivory in *Gorilla* (Remis, 1997). These differences in dietary habitat would also be related to enamel thickness and its distribution (Kono, 2004; Vogel et al., 2008). In the morphospace analyzed in this study, extant great apes and humans exhibit diversified morphologies (Figs. 3 and 4). It is likely that morphological diversification is associated with such specialization in the direction from centroid to taxon-specific clusters in the morphospace (Figs. 3 and 4). While such an adaptive scenario sounds reasonable, caution is warranted. Since form-function relationships of dp4

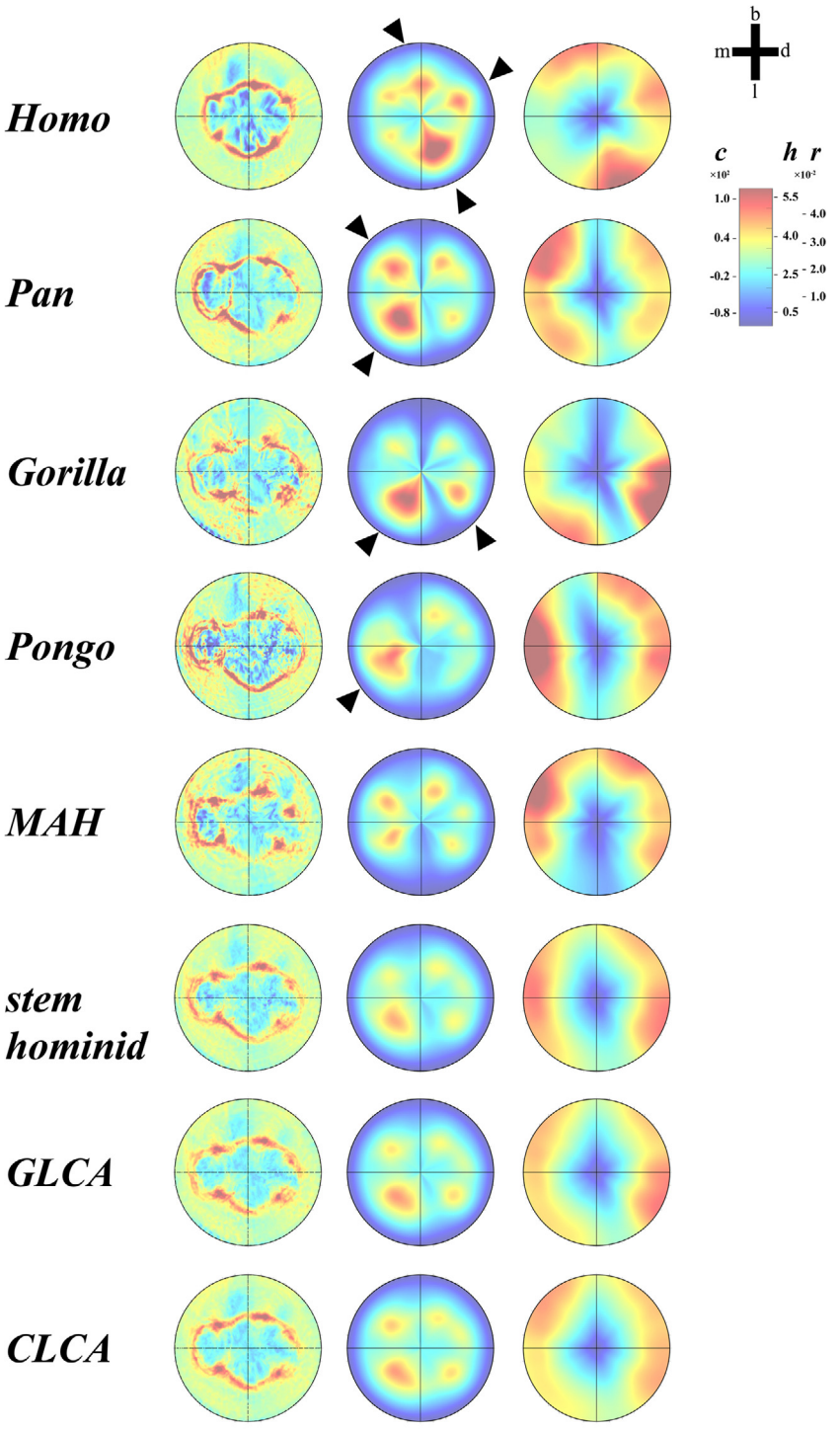

Fig. 8. Average morphometric maps (*c*, *h*, and *r* from left to right) of *Homo*, *Pan*, *Gorilla*, *Pongo*, and Early and Middle Miocene African Hominoids (MAH). The stem hominid, extant African ape and human ancestor (GLCA), and the chimpanzee/human last common ancestor (CLCA) were reconstructed from the inferred ancestral state using bgPC scores. Arrows indicate marked cusps (*Homo*: talonid, *Pan*: trigonid, *Gorilla*: lingual, *Pongo*: metaconid).
Fig. 8. Cartes morphométriques moyennes (*c*, *h*, et *r* de gauche à droite) de *Homo*, *Pan*, *Gorilla*, *Pongo* et d'hominoïdes africains du Miocène inférieur et moyen (MAH). L'hominidé souche, ancêtre africain des grands singes existants et des humains (GLCA) et le dernier ancêtre commun chimpanzé/humain (CLCA) ont été reconstruits à partir de l'état ancestral inféré en utilisant les résultats des bgPC. Les flèches indiquent les cuspides les plus marquées (*Homo* : talonide, *Pan* : trigonide, *Gorilla* : cuspides linguales, *Pongo* : métaconide).

morphology are yet to be investigated in detail, it remains elusive to what extent the taxon-specific dp4 morphologies reflect phylogenetic effects that are not directly related to functional adaptations.

In the context of interpreting the mandibular tooth morphology of *Ouranopithecus*, Koufos and de Bonis (2004) used the degree of "molarization" in dp4 as a criterion to determine primitive versus derived states. They suggested that a greater degree of molarization of dp4 (i.e., more molar-like dp4) indicates a derived feature. Further, they concluded that the dp4 of *Ouranopithecus* represents a derived state since it has a more molarized dp4 than chimpanzees and gorillas (see also Macchiarelli et al., 2009). Our MM-based approach shows a new perspective on evolutionary history. Fig. 8 shows that MAH in general have five cusps, which are similarly developed and low. The ancestral morphologies reconstructed as internal nodes also retain this hypothetical generalized five-cusp state. On the other hand, extant great apes and humans also show five cusps but each species exhibits specific cusps that are more developed than the others (*Homo*, talonid; *Pan*, trigonid; *Gorilla*, lingual; *Pongo*, metaconid). This indicates that each of the extant species evolved taxon-specific features independently from the generalized dp4 shape represented in MAH.

The MM-based PCA also gave insights into the evolution of dp4 morphology in hominins. Plio-Pleistocene *Australopithecus* and *Paranthropus* are not included in the range of extant hominids but occupied similar locations to the Miocene African hominoids in the morphospace (Figs. 3 and 4). This indicates that the deciduous teeth of Plio-Pleistocene hominins retain low-specialized morphology and are different from those of modern *Homo*, which show derived features. The robust australopiths (*Paranthropus*) have been traditionally considered to be specialized herbivores, consuming harder and relatively brittle food (Grine and Kay, 1988). Recent isotopic and dental microwear analyses, however, revealed their broad range of food resources in adulthood (Balter et al., 2012; Scott et al., 2005; Sponheimer and Lee-Thorp, 1999; Sponheimer et al., 2013).

Our data show that gracile and robust australopith individuals exhibit overall similar dp4 morphologies (Figs. 3 and 4). This contrasts with considerable differences of masticatory structures in gracile and robust australopiths. The similar dp4 EDJ morphology of *Australopithecus* and *Paranthropus* may reflect the evolutionary degree of conservation of deciduous teeth. It may also reflect genetic cohesiveness among southern African australopiths.

The *Nakalipithecus* specimen resembles Early and Middle Miocene African hominoids in the bgPC1 and bgPC2 axes (Fig. 3) and is located close to the central node of the neighbour-net diagram (Fig. 5). This indicates that *Nakalipithecus* retains dp4 ancestral morphology that is shared with earlier African fossil hominoids. These results suggest the African origin of *Nakalipithecus*. On the other hand, the *Ouranopithecus* specimen is far from the African Mio–Pliocene hominoid group, including *Nakalipithecus* and australopiths in Fig. 3, and is located more distant from the stem of the diagram (Fig. 5). This indicates that dp4 of *Ouranopithecus* is more derived than that of *Nakalipithecus*, though morphological similarities between *Nakalipithecus* and *Ouranopithecus* have found in size and some dentognathic features, such as mandible, permanent upper canine, and lower premolars (Kunimatsu et al., 2007). In fact, *Nakalipithecus* and *Ouranopithecus* specimens resemble each other along bgPC1 and bgPC3 (Fig. 4) and are located relatively close to each other in the neighbour-net diagram (Fig. 5). Assuming that this similarity and character state between them reflect phylogeny, *Nakalipithecus* could be a member of taxa from which the lineage to which *Ouranopithecus* belongs is derived. This "ancestral-descendant" relationship between *Nakalipithecus* and *Ouranopithecus* is consistent with the currently known chronology of these taxa (*Nakalipithecus*: 9.9–9.8 Ma, *Ouranopithecus*: 9.6–8.7 Ma). The alternative interpretation is convergence, i.e., the structural signal captured in this study indicates independent dietary adaptations in these taxa rather than phyletic history. If this were the case, then *Ouranopithecus* might be a relatively derived taxon among the Miocene Eurasian ape lineage. To draw more definitive conclusions on ape evolution during the Miocene, further analyses should be performed that encompass further data, especially on Eurasian hominids, such as dryopiths and *Sivapithecus*. In any case, morphological similarity among African fossils from Miocene hominoids to Plio-Pleistocene australopiths suggests that African apes maintain the phenotypic identity without genetic contribution from Eurasian lineages, which is consistent with the African origin hypothesis (H1) of AAH. Considering the ancestral state of morphology, locality, and chronology, *Nakalipithecus* may not be a direct ancestor itself but could be one of the stem species lineages for membership in the African great ape and human clade.

We analyzed the dp4 morphology of fossil and living hominids using novel geometric morphometric methods. Phenotypic continuity in African fossils from Miocene to Plio-Pleistocene indicated in this study is consistent with the African origin of AAH. Dental character states and moderate morphological similarity among *Nakalipithecus* and *Ouranopithecus* would reflect their "ancestral-descendant" relationship, but further comparative studies are needed to clarify phylogenetic relationship of Miocene apes.

Acknowledgements

This paper is a tribute to Laurent Puymerail, who has prematurely passed away, leaving a great contribution to the three-dimensional morphometric mapping in paleoanthropology. The authors thank G. Suwa, R. Kono, T. Domon and S. Takahashi for thoughtful discussion and comments. We are also grateful to Y. Kikuchi for collecting datasets. We thank L. de Bonis and R. Macchiarelli for having provided the μCT record of *Ouranopithecus macedoniensis* discussed in this paper. We also thank S. Potze for the access to the *Australopithecus* and *Paranthropus* specimens stored at the Ditsong National Museum of Natural History of Pretoria, South Africa, within the context of an ongoing research project led by J. Braga. We appreciate the Government of Kenya and the National Museums of Kenya for permitting us to examine fossil materials. We appreciate the assistance from the JSPS Nairobi Research Station during our research in Kenya. This work was in part supported by JSPS KAKENHI

Grant Nos. 18255006, 22255006, 24000015, 25257408, and 16H02757 to M.N., and 15H05609 to N.M.

Appendix A. Supplementary data

Supplementary data associated with this article can be found, in the online version, at http://dx.doi.org/10.1016/j.crpv.2016.10.004.

References

Agustí, J., Cabrera, L., Garcés, M., 2001. Chronology and zoogeography of the Miocene hominoid record in Europe. In: de Bonis, L., Koufos, G.D., Andrews, P. (Eds.), Hominoid Evolution and Environmental Change in the Neogene of Europe. Vol. 2. Phylogeny of the Neogene Hominoid Primates of Eurasia. Cambridge University Press, Cambridge, pp. 2–18.

Almécija, S., Smaers, J.B., Jungers, W.L., 2015. The evolution of human and ape hand proportions. Nat. Commun. 6, 7717.

Almécija, S., Tallman, M., Alba, D.M., Pina, M., Moyá-Solá, S., Jungers, W.L., 2013. The femur of *Orrorin tugenensis* exhibits morphometric affinities with both Miocene apes and later hominins. Nat. Commun. 4, 2888.

Andrews, P.J., Harrison, T., Delson, E., Bernor, R.L., Martin, L., 1996. Distribution and biochronology of European and Southwestern Asian Miocene catarrhines. In: Bernor, R.L., Fahlbusch, V., Mittmann, H.W. (Eds.), The Evolution of Western Eurasian Neogene Mammal Faunas. Columbia University Press, New York, pp. 168–295.

Arnold, C., Matthews, L.J., Nunn, C.L., 2010. The 10kTrees website: a new online resource for primate phylogeny. Evol. Anthropol. 19, 114–118.

Bailey, S.E., Benazzi, S., Buti, L., Hublin, J.-J., 2016. Allometry, merism and tooth shape of the lower second deciduous molar and first permanent molar. Am. J. Phys. Anthropol. 159, 93–105.

Bailey, S.E., Benazzi, S., Souday, C., Astorino, C., Paul, K., Hublin, J.-J., 2014. Taxonomic differences in deciduous upper second molar crown outlines of *Homo sapiens*, *Homo neanderthalensis* and *Homo erectus*. J. Hum. Evol. 72, 1–9.

Balter, V., Braga, J., Télouk, P., Thackeray, J.F., 2012. Evidence for dietary change but not landscape use in South African early hominins. Nature 489, 558–560.

Bayle, P., Macchiarelli, R., Trinkaus, E., Duarte, C., Mazurier, A., Zilhão, J., 2010. Dental maturational sequence and dental tissue proportions in the early Upper Paleolithic child from Abrigo do Lagar Velho, Portugal. Proc. Natl. Acad. Sci. U.S.A. 107, 1338–1342.

Begun, D.R., 1994. Relations among the great apes and humans: new interpretations based on the fossil great ape *Dryopithecus*. Yrbk. Phys. Anthropol. 37, 11–63.

Begun, D.R., 2001. African and Eurasian Miocene hominoids and the origins of the Hominidae. In: de Bonis, L., Koufos, G.D., Andrews, P. (Eds.), Phylogeny of the Neogene Hominoid Primates of Eurasia. Cambridge University Press, Cambridge, pp. 231–253.

Begun, D.R., 2002. European hominoids. In: Hartwig, W. (Ed.), The Primate Fossil Record. Cambridge University Press, Cambridge, pp. 339–368.

Begun, D.R., 2005. *Sivapithecus* is east and *Dryopithecus* is west, and never the twain shall meet. Anthropol. Sci. 113, 53–64.

Begun, D.R., 2007. Fossil record of Miocene hominoids. In: Henke, W., Tattersall, I. (Eds.), Handbook of Paleoanthropology, vol. 2. Springer, Berlin, pp. 921–977.

Begun, D.R., 2010. Miocene hominids and the origins of the African apes and humans. Annu. Rev. Anthropol. 39, 67–84.

Begun, D.R., Kordos, L., 1997. Phyletic affinities and functional convergence in *Dryopithecus* and other Miocene and living hominids. In: Begun, D.R., Ward, C.V., Rose, M.D. (Eds.), Function, Phylogeny and Fossils: Miocene Hominoid Evolution and Adaptations. Plenum Publishing Co., New York, pp. 291–316.

Begun, D.R., Nargolwalla, M.C., Kordos, L., 2012. European Miocene hominids and the origin of the African ape and human clade. Evol. Anthropol. 21, 10–23.

Benazzi, S., Douka, K., Fornai, C., Bauer, C.C., Kullmer, O., Svoboda, J., Pap, I., Mallegni, F., Bayle, P., Coquerelle, M., Condemi, S., Ronchitelli, A., Harvati, K., Weber, G.W., 2011b. Early dispersal of modern humans in Europe and implications for Neanderthal behaviour. Nature 479, 525–528.

Benazzi, S., Fornai, C., Bayle, P., Coquerelle, M., Kullmer, O., Mallegni, F., Weber, G.W., 2011a. Comparison of dental measurement systems for taxonomic assignment of Neanderthal and modern human lower second deciduous molars. J. Hum. Evol. 61, 320–326.

Bockmann, M.R., Hughes, T.E., Townsend, G., 2010. Genetic modeling of primary tooth emergence: a study of Australian twins. Twin Res. Hum. Gen. 13, 573–581.

Bolk, L., 1916. Problems of human dentition. Am. J. Anat. 19, 91–148.

Bookstein, F.L., 1991. Morphometric Tools for Landmark Data: Geometry and Biology. Cambridge University Press, Cambridge.

Butler, P.M., 1956. The ontogeny of molar pattern. Biol. Rev. 31, 30–70.

Butler, P.M., 1971. Growth of human tooth germs. In: Dahlberg, A.A. (Ed.), Dental Morphology and Evolution. University of Chicago Press, Chicago, pp. 3–14.

Coleman, M.N., Colbert, M.W., 2007. Technical note: CT thresholding protocols for taking measurements on three-dimensional models. Am. J. Phys. Anthropol. 133, 723–725.

Dahlberg, A.A., 1945. The changing dentition of man. J. Am. Dent. Assoc. 32, 676–690.

de Bonis, L., Bouvrain, G., Geraads, D., Koufos, G., 1990. New hominid skull material from the late Miocene of Macedonia in northern Greece. Nature 345, 712–714.

de Bonis, L., Koufos, G., 1993. The face and mandible of *Ouranopithecus macedoniensis*: description of new specimens and comparisons. J. Hum. Evol. 24, 469–491.

de Bonis, L., Koufos, G., 1994. Our ancestors' ancestor: *Ouranopithecus* is a Greek link in human ancestry. Evol. Anthropol. 3, 75–83.

de Bonis, L., Koufos, G., 1997. The phylogenetic and functional implications of *Ouranopithecus macedoniensis*. In: Begun, D.R., Ward, C.V., Rose, M.D. (Eds.), Function, Phylogeny and Fossils: Miocene Hominoid Evolution and Adaptations. Plenum Publishing Co., New York, pp. 317–326.

de Bonis, L., Melentis, J., 1977. Les Primates hominoïdes du Vallésien de Macédoine (Grèce). Etude de la mâchoire inférieure. Geobios 10, 849–885.

Evans, A.R., Daly, E.S., Catlett, K.K., Paul, K.S., King, S.J., Skinner, M.M., Nesse, H.P., Hublin, J.-J., Townsend, G.C., Schwartz, G.T., Jernvall, J., 2016. A simple rule governs the evolution and development of hominin tooth size. Nature 530, 477–480.

Fajardo, R.J., Ryan, T.M., Kappelman, J., 2002. Assessing the accuracy of high-resolution X-ray computed tomography of primate trabecular bone by comparisons with histological sections. Am. J. Phys. Anthropol. 118, 1–10.

Gómez-Robles, A., de Castro, J.M.B., Martinón-Torres, M., Prado-Simón, L., Arsuaga, J.L., 2012. A geometric morphometric analysis of hominin upper second and third molars, with particular emphasis on European Pleistocene populations. J. Hum. Evol. 63, 512–526.

Gómez-Robles, A., de Castro, J.M.B., Martinón-Torres, M., Prado-Simón, L., Arsuaga, J.L., 2015. A geometric morphometric analysis of hominin lower molars: evolutionary implications and overview of postcanine dental variation. J. Hum. Evol. 82, 34–50.

Grine, F.E., Kay, R.F., 1988. Early hominid diets from quantitative image analysis of dental microwear. Nature 333, 765–768.

Gunz, P., Neubauer, S., Golovanova, L., Doronichev, V., Maureille, B., Hublin, J.-J., 2012. A uniquely modern human pattern of endocranial development. Insights from a new cranial reconstruction of the Neandertal newborn from Mezmaiskaya. J. Hum. Evol. 62, 300–313.

Guy, F., Gouvard, F., Boistel, R., Euriat, A., Lazzari, V., 2013. Prospective in (primate) dental analysis through tooth 3D topographical quantification. PLoS ONE 8, e66142.

Hull, P.M., Darroch, S.A.F., Erwin, D.H., 2015. Rarity in mass extinctions and the future of ecosystems. Nature 528, 345–351.

Huson, D.H., Bryant, D., 2006. Application of phylogenetic net-works in evolutionary studies. Mol. Biol. Evol. 23, 254–267.

Ishida, H., Pickford, M., 1997. A new late Miocene hominoid from Kenya: *Samburupithecus kiptalami* gen. et sp. nov. C. R. Acad. Sci. Paris, Ser. D 325, 823–829.

Janmaat, K.R.L., Boesch, C., Byrne, R., Chapman, C.A., Goné Bi, Z.B., Head, J.S., Robbins, M.M., Wrangham, R.W., Polansky, L., 2016. Spatio-temporal complexity of chimpanzee food: how cognitive adaptations can counteract the ephemeral nature of ripe fruit. Am. J. Primatol. 78, 626–645.

Jernvall, J., Jung, H.S., 2000. Genotype, phenotype, and developmental biology of molar tooth characters. Yrbk. Phys. Anthropol. 43, 171–190.

Jernvall, J., Thesleff, I., 2012. Tooth shape formation and tooth renewal: evolving with the same signals. Development 139, 3487–3497.

Katoh, S., Beyene, Y., Itaya, T., Hyodo, H., Hyodo, M., Yagi, K., Gouzu, C., WoldeGabriel, G., Hart, W.K., Ambrose, S.H., Nakaya, H., Bernor, R.L., Boisserie, J.-R., Bibi, F., Saegusa, H., Sasaki, T., Sano, K., Asfaw, B., Suwa, G., 2016. New geological and palaeontological age constraint for the gorilla–human lineage split. Nature 530, 215–218.

Kono, R.T., 2004. Molar enamel thickness and distribution patterns in extant great apes and humans: new insights based on a 3-dimensional whole crown perspective. Anthropol. Sci. 112, 121–146.

Korenhof, C.A.W., 1960. Morphogenetical Aspects of the Human Upper Molar. Uitgeversmaatschappij Neerlandia, Utrecht, 368 p.
Koufos, G.D., 2007. Potential hominoid ancestors for Hominidae. In: Henke, W., Tattersall, I. (Eds.), Handbook of Palaeoanthropology. Vol. 3. Phylogeny of Hominids. Springer, Berlin, pp. 1347–1377.
Koufos, G.D., de Bonis, L., 2004. The deciduous lower dentition of *Ouranopithecus macedoniensis* (Primates, Hominoidea) from the Late Miocene deposits of Macedonia, Greece. J. Hum. Evol. 46, 699–718.
Kraus, B.S., 1952. Morphologic relationships between enamel and dentin surfaces of lower first molar teeth. J. Dent. Res. 31, 248–256.
Kraus, B.S., Jordan, R.E., 1965. The Human Dentition Before Birth. Lea and Febiger, Philadelphia, 218 p.
Kuhl, F.P., Giardina, C.R., 1982. Elliptic Fourier features of a closed contour. Comput. Graph. Image Process. 18, 236–258.
Kunimatsu, Y., Nakatsukasa, M., Sawada, Y., Sakai, T., Hyodo, M., Hyodo, H., Itaya, T., Nakaya, H., Saegusa, H., Mazurier, A., Saneyoshi, M., Tsujikawa, H., Yamamoto, A., Mbual, E., 2007. A new Late Miocene great ape from Kenya and its implications for the origins of African great apes and humans. Proc. Natl. Acad. Sci. U.S.A. 104, 19220–19225.
Kunimatsu, Y., Nakatsukasa, M., Sawada, Y., Sakai, T., Saneyoshi, M., Yamamoto, A., Mbual, E., 2016. A second hominoid species in the early Late Miocene fauna of Nakali (Kenya). Anthropol. Sci. 124, 75–83.
Lovejoy, C.O., Suwa, G., Simpson, S.W., Matternes, J.H., White, T.D., 2009. The great divides: *Ardipithecus ramidus* reveals the postcrania of our last common ancestors with African apes. Science 326, 100–106.
Macchiarelli, R., Bayle, P., Bondioli, L., Mazurier, A., Zanolli, C., 2013. From outer to inner structural morphology in dental anthropology. The integration of the third dimension in the visualization and quantitative analysis of fossil remains. In: Scott, R.G., Irish, J.D. (Eds.), Anthropological Perspectives on Tooth Morphology: Genetics, Evolution, Variation. Cambridge University Press, Cambridge, pp. 250–277.
Macchiarelli, R., Bondioli, L., Debénath, A., Mazurier, A., Tournepiche, J.F., Birch, W., Dean, C., 2006. How Neanderthal molar teeth grew. Nature 444, 748–751.
Macchiarelli, R., Bondioli, L., Falk, D., Faupl, P., Illerhaus, B., Kullmer, O., Richter, W., Said, H., Sandrock, O., Schäfer, K., Urbanek, C., Viola, B.T., Weber, G.W., Seidler, H., 2004. Early Pliocene hominid tooth from Galili, Somali Region, Ethiopia. Coll. Antropol. 28, 65–76.
Macchiarelli, R., Mazurier, A., Illerhaus, B., Zanolli, C., 2009. *Ouranopithecus macedoniensis* (Mammalia, Primates, Hominoidea): virtual reconstruction and 3D analysis of a juvenile mandibular dentition (RPl-82 and RPl-83). Geodiversitas 31, 851–864.
Maddison, W.P., Maddison, D.R., 2015. Mesquite: A Modular System for Evolutionary Analysis. v3.03, mesquiteproject.org.
Mitteroecker, P., Bookstein, F., 2011. Linear discrimination, ordination, and the visualization of selection gradients in modern morphometrics. Evol. Biol. 38, 100–114.
Morimoto, N., Ponce de León, M.S., Zollikofer, C.P.E., 2014. Phenotypic variation in infants, not adults, reflects genotypic variation among chimpanzees and bonobos. PLOS ONE 9, e102074.
Morimoto, N., Zollikofer, C.P.E., Ponce de León, M.S., 2011. Exploring femoral diaphyseal shape variation in wild and captive chimpanzees by means of morphometric mapping: a test of Wolff's Law. Anat. Rec. 294, 589–609.
Morimoto, N., Zollikofer, C.P.E., Ponce de León, M.S., 2012. Shared human–chimpanzee pattern of perinatal femoral shaft morphology and its implications for the evolution of hominin locomotor adaptations. PLoS ONE 7, e41980.
Morita, W., Morimoto, N., Ohshima, H., 2016. Exploring metameric variation in human molars: a morphological study using morphometric mapping. J. Anat. 229, 343–355.
Morita, W., Yano, W., Nagaoka, T., Abe, M., Ohshima, H., Nakatsukasa, M., 2014. Patterns of morphological variation in enamel–dentin junction and outer enamel surface of human molars. J. Anat. 224, 669–680.
Moyá-Solá, M., Köhler, M., 1995. New partial cranium of *Dryopithecus* Lartet, 1863 (Hominoidea, Primates) from the upper Miocene of Can Llobateres, Barcelona, Spain. J. Hum. Evol. 29, 101–139.
Moyá-Solá, S., Alba, D.M., Almécija, S., Casanovas-Vilar, I., Köhler, M., De Esteban-Trivigno, S., Robles, J.M., Galindo, J., Fortuny, J., 2009. A unique Middle Miocene European hominoid and the origins of the great ape and human clade. Proc. Natl. Acad. Sci. U.S.A. 106, 9601–9606.
Nakatsukasa, M., Kunimatsu, Y., 2009. *Nacholapithecus* and its importance for understanding hominoid evolution. Evol. Anthropol. 18, 103–119.
Nanci, A., 2013. Ten Cate's Oral Histology: Development, Structure, and Function, 8th ed. Elsevier Health Sciences, St. Louis, 411 p.
Olejniczak, A.J., Gilbert, C.G., Martin, L.B., Smith, T.M., Ulhaas, L., Grine, F.E., 2007. Morphology of the enamel–dentine junction in sections of anthropoid primate maxillary molars. J. Hum. Evol. 53, 292–301.
Pilbrow, V., 2007. Patterns of molar variation in great apes and their implications for hominin taxonomy. In: Bailey, S.E., Hublin, J.-J. (Eds.), Dental Perspectives on Human Evolution: State of the Art Research in Dental Anthropology. Springer Netherlands, Dordrecht, pp. 9–32.
Puymerail, L., Ruff, C.B., Bondioli, L., Widianto, H., Trinkaus, E., Macchiarelli, R., 2012. Structural analysis of the Kresna 11 *Homo erectus* femoral shaft (Sangiran, Java). J. Hum. Evol. 63, 741–749.
Remis, M.J., 1997. Western lowland gorillas (*Gorilla gorilla gorilla*) as seasonal frugivores: use of variable resources. Am. J. Primatol. 43, 87–109.
Revell, L.J., 2012. Phytools: an R package for phylogenetic comparative biology (and other things). Methods Ecol. Evol. 3, 217–223.
Saunders, S.R., Mayhall, J.T., 1982. Developmental patterns of human morphological traits. Arch. Oral Biol. 27, 45–49.
Scott, R.S., Bergstrom, T.S., Brown, C.A., Grine, F.E., Teaford, M.F., Walker, A., Ungar, P.S., 2005. Dental microwear texture analysis shows within species diet variability in fossil hominins. Nature 436, 693–695.
Skinner, M.M., Alemseged, Z., Gaunitz, C., Hublin, J.-J., 2015. Enamel thickness trends in Plio-Pleistocene hominin mandibular molars. J. Hum. Evol. 85, 35–45.
Skinner, M.M., de Vries, D., Gunz, P., Kupczik, K., Klassen, R.P., Hublin, J.-J., Roksandic, M., 2016. A dental perspective on the taxonomic affinity of the Balanica mandible (BH-1). J. Hum. Evol. 93, 63–81.
Skinner, M.M., Evans, A., Smith, T.M., Jernvall, J., Tafforeau, P., Kupczik, K., Olejniczak, A.J., Rosas, A., Radovcic, J., Thackeray, J.F., Toussaint, M., Hublin, J.-J., 2010. Contributions of enamel–dentine junction shape and enamel deposition to primate molar crown complexity. Am. J. Phys. Anthropol. 142, 157–163.
Skinner, M.M., Gunz, P., Wood, B.A., Boesch, C., Hublin, J.-J., 2009a. Discrimination of extant *Pan* species and subspecies using the enamel–dentine junction morphology of lower molars. Am. J. Phys. Anthropol. 140, 234–243.
Skinner, M.M., Wood, B.A., Boesch, C., Olejniczak, A.J., Rosas, A., Smith, T.M., Hublin, J.-J., 2008. Dental trait expression at the enamel–dentine junction of lower molars in extant and fossil hominoids. J. Hum. Evol. 54, 173–186.
Skinner, M.M., Wood, B.A., Hublin, J.-J., 2009b. Protostylid expression at the enamel–dentine junction and enamel surface of mandibular molars of *Paranthropus robustus* and *Australopithecus africanus*. J. Hum. Evol. 56, 76–85.
Smith, P., 1989. Dental evidence for phylogenetic relationships of Middle Paleolithic hominids. In: Otte, M. (Ed.), L'Homme de Néandertal. Université de Liège, Liège, pp. 111–120.
Smith, P., Gomori, J.M., Shaked, R., Haydenblit, R., Joskowicz, L., 2000. A computerized approach to reconstruction of growth patterns in hominid molar teeth. In: Mayhall, J., Heikkinen, T. (Eds.), Proceedings of the 11th International Symposium on Dental Morphology. Oulu University Press, Oulu, pp. 388–397.
Smith, P., Gomorri, J.M., Spitz, S., Becker, J., 1997. Model for the examination of evolutionary trends in tooth development. Am. J. Phys. Anthropol. 102, 283–294.
Smith, P., Tillier, A.M., 1989. Additional infant remains from the Mousterian Strata, Kebara Cave (Israel). In: Bar-Yosef, O., Vandermeersch, B. (Eds.), Investigation in South Levantine Prehistory. British Archaeological Reports International Series. Archaeopress, Oxford, pp. 323–335.
Smith, T.M., Tafforeau, P., 2008. New visions of dental tissue research: tooth development, chemistry, and structure. Evol. Anthropol. 17, 213–226.
Smith, T.M., Toussaint, M., Reid, D.J., Olejniczak, A.J., Hublin, J.J., 2007. Rapid dental development in a Middle Paleolithic Belgian neanderthal. Proc. Natl. Acad. Sci. U.S.A. 104, 20220–20225.
Sponheimer, M., Alemseged, Z., Cerling, T.E., Grine, F.E., Kimbel, W.H., Leakey, M.G., Lee-Thorp, J.A., Manthi, F.K., Reed, K.E., Wood, B.A., Wynn, J.G., 2013. Isotopic evidence of early hominin diets. Proc. Natl. Acad. Sci. U.S.A. 110, 10513–10518.
Sponheimer, M., Lee-Thorp, J.A., 1999. Isotopic evidence for the diet of an early hominid, *Australopithecus africanus*. Science 283, 368–370.
Spoor, C.F., Zonneveld, F.W., Macho, G.A., 1993. Linear measurements of cortical bone and dental enamel by computed tomography: applications and problems. Am. J. Phys. Anthropol. 91, 469–484.
Suwa, G., Kono, R.T., Katoh, S., Asfaw, B., Beyene, Y., 2007. A new species of great ape from the late Miocene epoch in Ethiopia. Nature 448, 921–924.
Suwa, G., Kono, R.T., Simpson, S.W., Asfaw, B., Lovejoy, C.O., White, T.D., 2009. Paleobiological implications of the *Ardipithecus ramidus* dentition. Science 326, 69–99.
Suzuki, M., Sakai, T., 1973. Occlusal surface pattern of the lower molars and the second deciduous molar among living Polynesians. Am. J. Phys. Anthropol. 39, 305–315.

Vogel, E.R., van Woerden, J.T., Lucas, P.W., Atmoko, S.S.U., van Schaik, C.P., Dominy, N.J., 2008. Functional ecology and evolution of hominoid molar enamel thickness: *Pan troglodytes schweinfurthii* and *Pongo pygmaeus wurmbii*. J. Hum. Evol. 55, 60–74.

Yamagiwa, J., Basabose, A.K., 2006. Diet and seasonal changes in sympatric gorillas and chimpanzees at Kahuzi-Biega National Park. Primates 47, 74–90.

Zanolli, C., 2015. Molar crown inner structural organization in Javanese *Homo erectus*. Am. J. Phys. Anthropol. 156, 148–157.

Zanolli, C., Mazurier, A., 2013. Endostructural characterization of the *H. heidelbergensis* dental remains from the early Middle Pleistocene site of Tighenif, Algeria. C. R. Palevol 12, 293–304.

Zanolli, C., Bayle, P., Macchiarelli, R., 2010. Tissue proportions and enamel thickness distribution in the early Middle Pleistocene human deciduous molars from Tighenif, Algeria. C. R. Palevol 9, 341–348.

Zanolli, C., Bondioli, L., Coppa, A., Dean, C.M., Bayle, P., Candilio, F., Capuani, S., Dreossi, D., Fiore, I., Frayer, D.W., Libsekal, Y., Mancini, L., Rook, L., Tekle, T.M., Tuniz, C., Macchiarelli, R., 2014. The late Early Pleistocene human dental remains from Uadi Aalad and Mulhuli-Amo (Buia), Eritrean Danakil: macromorphology and microstructure. J. Hum. Evol. 74, 96–113.

Zanolli, C., Bondioli, L., Mancini, L., Mazurier, A., Widianto, H., Macchiarelli, R., 2012. Two human fossil deciduous molars from the Sangiran Dome (Java, Indonesia): outer and inner morphology. Am. J. Phys. Anthropol. 147, 472–481.

Zanolli, C., Dean, M.C., Rook, L., Bondioli, L., Mazurier, A., Macchiarelli, R., 2016. Enamel thickness and enamel growth in *Oreopithecus*: combining microtomographic and histological evidence. C. R. Palevol 15, 209–226.

Zanolli, C., Grine, F.E., Kullmer, O., Schrenk, F., Macchiarelli, R., 2015. The Early Pleistocene deciduous hominid molar FS-72 from the Sangiran Dome of Java, Indonesia: a taxonomic reappraisal based on its comparative endostructural characterization. Am. J. Phys. Anthropol. 157, 666–674.